Heiska, Juho; Sorsa, Olli; Kallio, Tanja; Karppinen, Maarit

Benzenedisulfonic Acid as an ALD/MLD Building Block for Crystalline Metal-Organic Thin Films**

Benzenedisulfonic Acid as an ALD/MLD Building Block for Crystalline Metal-Organic Thin Films**

Juho Heiska,[a] Olli Sorsa,[a] Tanja Kallio,[a] and Maarit Karppinen*[a]

Abstract: Two new atomic/molecular layer deposition processes for depositing crystalline metal-organic thin films, built from 1,4-benzenedisulfonate (BDS) as the organic linker and Cu or Li as the metal node, are reported. The processes yield in-situ crystalline but hydrated Cu-BDS and Li-BDS films; in the former case, the crystal structure is of a previously known metal-organic-framework-like structure, while in the latter case not known from previous studies. Both hydrated materials can be readily dried to obtain the crystalline unhydrated phases. The stability and the ionic conductivity of the unhydrated Li-BDS films were characterized to assess their applicability as a thin film solid polymer Li-ion conductor.

Introduction

Atomic layer deposition (ALD) has been already for years the fastest-growing thin-film deposition technology in microelectronics,[1,2] but it is gaining attention in energy applications as well, including the lithium-ion battery (LIB) field.[3,4] Molecular layer deposition (MLD) is a much less exploited counterpart of ALD for organic thin films.[2,5] Combining these two methods into ALD/MLD allows the deposition of metal-organic films. In the LIB field, all these methods are used, especially in the contexts of the micro-battery,[6] inorganic solid electrolyte (ISE), solid polymer electrolyte (SPE), and electrode-electrolyte interface design.[3,7–13] In particular, ALD/MLD has been exploited to modify the electrode/electrolyte interfaces to improve the cycle life of the battery.[14–17]

A prototype SPE is a polyethylene oxide mixed with lithium salt. The lithium salt is needed to enhance the poor ionic conductivity of the SPE, but the drawback is that it at the same time tends to deteriorate the electrochemical stability of the SPE material.[18] On the other hand, the SPEs win out in processability and flexibility, suffer less from interfacial resistance, and are cheaper to manufacture compared to the ISEs.[19,20] Recently, a new type of SPE has regained research interest, so-called solid polymeric single Li-ion conductor (SPSLIC).[21] A SPSLIC material is based on immobilized anions such as Li-sulfonates. Since the anions are immobilized, the

lithium transference number is usually larger than in SPEs and closer to unity. These materials are also electrochemically stable, and – according to theoretical calculations – can effectively reduce the Li-ion concentration gradient in Li plating/stripping.[21,22] However, the most significant drawback of SPSLICs is still their low ionic conductivity compared to the ISEs and SPEs. This is due to the strong association between the sulfonate and the lithium ion. To overcome the problem, SPSLICs are often polymerized e.g. in a polyethylene oxide matrix or with other oligomers that can dissociate the Li+ ion to make it more mobile.[23–25]

The only SPSLIC-type materials deposited with ALD/MLD are aliphatic lithium compounds.[12,26,27] Here we like to propose dilithium-1,4-benzenedisulfonate (Li-BDS) as a relatively simple SPSLIC and possibly attainable through ALD/MLD synthesis. Interestingly, the prospective precursor for BDS in ALD/MLD, 1,4-benzenedisulfonic acid (HBDS), shares many chemical properties with terephthalic acid (TPA; 1,4-benzenedicarboxylic acid), which is one of the most common MLD precursors and is known to readily react with metal-bearing ALD precursors to form stable crystalline metal-organic thin films, somewhat similar to metal-organic framework (MOF) structures.[28–36] Hence, we consider HBDS as an interesting analog to TPA in ALD/MLD. It is significantly (approx. six orders of magnitude)[37] more acidic than TPA, which could enable the use of less reactive inorganic precursors. For some MOFs replacing the TPA linker with BDS considerably enhances the thermal stability, e.g. from ca. 200 to ca. 400°C for the Cu-TPA versus Cu-BDS.[38,39] So far in the literature, considerably fewer BDS-based MOFs have been reported compared to the extensive literature on metal carboxylates.
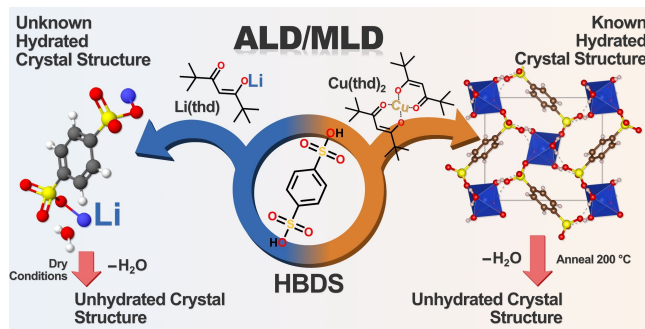
In this article, we report new ALD/MLD processes for two metal 1,4-benzenedisulfonate materials, Cu-BDS and Li-BDS, see Figure 1. The former compound was chosen as its crystal structure was known from solution-synthesized bulk samples[39] and it had shown some promise as a matrix for sulfur infiltration in Li–S batteries, implying some degree of porosity.[40] The latter Li-BDS compound, which we consider as the main candidate for the new SPSLIC material, has been only briefly mentioned in

[a] J. Heiska, Dr. O. Sorsa, Prof. T. Kallio, Prof. M. Karppinen
Department of Chemistry and Materials Science
Aalto University
00076 Espoo (Finland)
E-mail: maarit.karppinen@aalto.fi

Chemistry–A European Journal

Full Paper
doi.org/10.1002/chem.202100538

Chemistry
Europe
European Chemical
Societies Publishing

**Figure 1.** Schematics of the present ALD/MLD processes and the resultant products.

literature without any in-depth discussion or reported XRD pattern.[41] The Li-BDS films turned out to be hygroscopic, exhibiting different crystalline forms depending on whether being hydrated or dehydrated. We investigate the thermal and electrochemical stabilities of these films and assess their ionic conductivity using AC impedance measurements.

Results and Discussion

The experimental can be found in Supporting Information. All the relevant process parameters, precursor synthesis, and descriptions of electrochemical setups are found within.

Cu-BDS ALD/MLD process

The Cu(thd)$_2$ + HBDS process experiments were carried out at 210 °C based on our preliminary tests. In the inset of Figure 2 we show the so-called growth-per-cycle (GPC) as a function of the precursor pulse length, for both precursors separately. This is the data needed to show that the surface reactions saturate. From Figure 2, for Cu(thd)$_2$ a pulse time of 4 s is enough while a
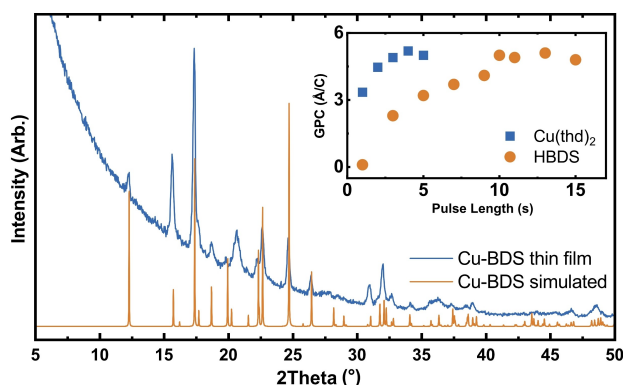
Figure 2. GIXRD pattern for as-deposited hydrated Cu-BDS film compared with the calculated XRD pattern based on the structure reported for Cu-BDS in bulk samples.[39] Inset shows the pulse saturation of the Cu(thd)$_2$ + HBDS ALD/MLD process at 210 °C.
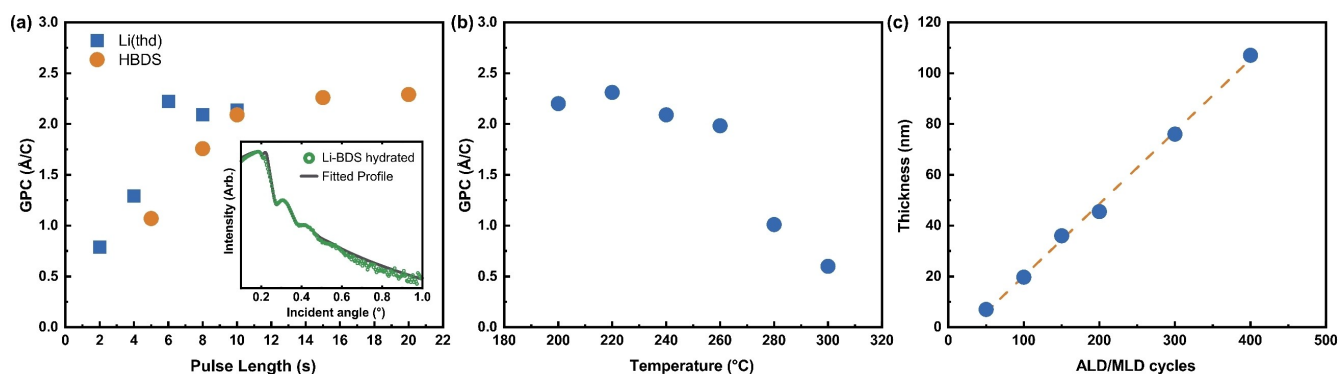
somewhat longer pulse time of 10 s is required for HBDS, which is typical for organic precursors in our reactor setup.[32,34,42] The process yields well-crystalline Cu-BDS films for which the post-deposition GIXRD analysis typically showed the presence of water of hydration. However, in very dry ambient humidity conditions it was possible to observe the unhydrated phase as well in the as-deposited films, which was then quickly hydrated unless properly protected. The water could also be afterwards removed by annealing (see FTIR and GIXRD data in Figures S1 and S2). The GIXRD pattern shown in Figure 2 is for a typical as-deposited Cu-BDS film and matches perfectly with the simulated XRD pattern based on the structure data reported for hydrated Cu-BDS,[39] evidencing the first ALD/MLD grown MOF-type thin film based on the BDS linker. Annealing the film removes the crystal water; the film remains crystalline, but the GIXRD pattern consists of few broad peaks only (Figure S2).

Li-BDS ALD/MLD process

Inspired by the success with the Cu(thd)$_2$ + HBDS process, we proceeded with the Li(thd) + HBDS process. The ALD/MLD parameters were found to be very similar for the two processes, with somewhat lower GPC values for the latter process (Figure 3). Very similar precursor pulse lengths were required again for saturation: 6 s for Li(thd) and 10 s for HBDS. The relatively large roughness of the films (e.g. 4 nm for a 30-nm thick film, typical for crystalline ALD/MLD Li-organic films[33,34]) made the fitting of the XRR data challenging. Therefore, the thicknesses of the films grown with 300 and 400 cycles were determined from cross-sectional SEM images (Figure S3). The dependence of the growth rate on the deposition temperature is depicted in Figure 3b, showing that with increasing temperature GPC remains essentially constant up to 260 °C (2.3 to 2.0 Å/cycle). Above 260 °C, the GPC rapidly decreases which is rather typical behavior for ALD/MLD processes.[28,29,32,33] We also confirmed the linear dependence of the film thickness on the number of ALD/MLD cycles (except the short "incubation period" in the beginning; Figure 3c). This type of incubation period is often seen with crystalline MOF-like structures,[30,32–34] while it is much more imperceptible with amorphous MOF-like materials that are deposited with ALD/MLD.[43] Finally, we determined the density of our as-deposited (hydrated) Li-BDS films to be 1.63 g/cm^3 based on XRR.

Chemical stability

Typically, the sulfonates are much more hygroscopic than their acid analogs.[39,44] The hygroscopicity was quite apparent for our Li-BDS films as well, which – without an exception – were received from the deposition reactor in their hydrated form (showing the characteristic –OH vibrations in FTIR spectra). The source of hydration is very likely the ambient humidity. Interestingly, the hydrated water simply disappeared when the films were stored for few hours in a desiccator. Both the as-deposited hydrated films and the post-deposition dehydrated

Chemistry–A European Journal

Full Paper
doi.org/10.1002/chem.202100538

Chemistry Europe
European Chemical
Societies Publishing

Figure 3. ALD/MLD parameter optimization for the Li(thd)+HBDS process: (a) GPC dependency on the precursor pulse lengths (100 ALD/MLD cycles; 200 °C), the inset showing the XRR spectrum with a fit, (b) GPC dependency on the deposition temperature (100 cycles), and (c) growth linearity at optimized conditions (200 °C, 6 s Li(thd) and 10 s HBDS). In (c) the points with 300 and 400 ALD/MLD cycles are estimations based on cross-sectional SEM images of the films (Figure S1).

films were crystalline, but the crystal structures are different as seen both from the GIXRD and FTIR data (Figure 4).

Upon the dehydration, the film density (determined from the critical angle in the XRR pattern) decreases, and the surface roughness slightly increases. In SEM images (Figure 4c), we can see that also the morphology changes upon the water release. The as-deposited water-containing film shows small crystallites typical to other crystalline ALD/MLD grown Li-organic films;[35] the cracks seen in the image are most probably caused by escaping water from the film while it is imaged under vacuum. For the unhydrated film, rather unique surface morphology is seen consisting of long crystal pillars.

The easy dehydration made the characterization somewhat challenging, as it was impossible to verify exactly the degree of (de)hydration. After the dehydration, the films were found somewhat resistant towards rehydration, as sometimes a mixture of both phases was seen in GIXRD (Figure S5). The Li-BDS films were stable at least up to 1 h anneal at 350 °C in the air or in a vacuum. At 400 °C some decomposition began (detected with FTIR), in a manner analogous to that of Cu-BDS, presumably due to the evolution of sulfurdioxide.[44] When

annealing at 450 °C in the air for 1 h the films changed visually as did the FTIR spectrum and GIXRD pattern and the structure was certainly decomposed. Hence, in this case (opposite to the Cu-BDS versus Cu-TPA case) the decomposition temperature is somewhat lower for Li-BDS than for Li-TPA (500 °C for 1 h),[33] underlining the fact that the thermal stability may depend also on the metal node.

FTIR analysis

A detailed discussion of the FTIR spectrum is found in the Supporting Information. The water of hydration is readily detected in the FTIR from the −OH stretching and bending modes around 3540 and 1640 cm^{-1}, respectively. The FTIR spectrum of aromatic sulfonates is often very similar in the range of 1300–1000 cm^{-1} consisting of four intense bands (roman numerals I–IV) due to $\nu_{as}(SO_3)$, $\nu(C-S)$, $\nu_s(SO_3)$, and $\nu(ring)$,[45] see Figure 4b. The FTIR spectra of Li-BDS and Cu-BDS are indeed very similar and the assignments for Li-BDS are easily transferable to Cu-BDS. The most notable difference is
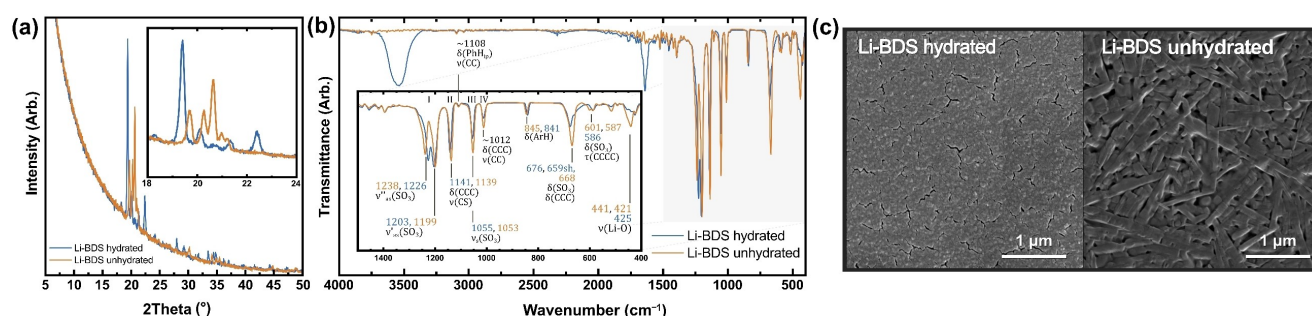
Figure 4. (a) GIXRD patterns of hydrated and unhydrated Li-BDS films (800 cycles at 200 °C). Inset shows a magnification between 18° and 24° to highlight the differences in the pattern. (b) Representative FTIR spectra of hydrated (800 cycles at 200 °C) and unhydrated Li-BDS spectra with inset highlighting the minor differences in the 1500 to 400 cm^{-1} range. Peak interpretation of the FTIR spectra is also included in the inset with blue (Li-BDS hydrated) and orange (Li-BDS unhydrated) color coding listing the wavenumbers. The roman numerals I–IV highlight the most typical peaks of metal-BDS compounds. A detailed discussion of the FTIR spectrum can be found in the Supporting Information. The symbols are ν for stretch, δ for bending, and τ for torsion. (c) SEM images of the Li-BDS films. Hydrated film is imaged directly after deposition while the unhydrated sample was stored in desiccator for 24 h prior imaging.

Chemistry—A European Journal

Full Paper
doi.org/10.1002/chem.202100538

Chemistry Europe
European Chemical
Societies Publishing

the splitting of ν_{as} in Cu-BDS $\Delta\nu_{as}$ is much larger (62 versus 39 cm^{-1}) indicating that Cu-BDS is more degenerate. Overall, our FTIR peaks correspond well to the expected vibrations for Li-BDS and Cu-BDS. Additional comparison of the ATR-FTIR spectra of the HBDS precursor and the hydrated Li-BDS film (Figure S4) confirms that the precursors have indeed fully reacted.

Electrochemical measurements

The ionic conductivity was measured in-plane for a 100 nm thick Li-BDS film deposited on interdigitated platinum electrodes (DropSens); a precise description of this setup can be found in Ref.[46] and the calculations for the conductivity in Supporting Information. The fitted impedance spectra are shown in Figure 5a with the relevant equivalent circuit,[47] and the resultant Arrhenius plot of conductivity and calculated activation energy in Figure 5b. At low temperature (RT-60°C), no EIS resulting from ionic conductivity was produced but at elevated temperatures of 80 and 118°C, decent ionic conductivity values of $4.1\cdot10^{-9}$ and $6.4\cdot10^{-8}$ S/cm, respectively, were determined. These values are low but comparable to those reported for the closest analog, i.e. $2.1\cdot10^{-8}$ S/cm at 70°C for amorphous poly(4-lithium styrene sulfonate).[24] The high activation energy value of 0.9 eV found for Li-BDS is a clear indication that conduction is intrinsic where defects are induced due to an increase in temperature.

Cyclic voltammetry experiments were carried out in cells with liquid electrolyte (Supporting Information). The results revealed little (to no) electroactivity compared to the blank reference. This is expected since sulfonates are known to be electrochemically quite stable.[21] During the 1st cycle there is a small reduction peak at 0.75 V, which could simply be due to a different kind of SEI formation compared to the reference. The large peak at 4.25 V is due to the oxidation of the liquid electrolyte. Therefore, as the oxidation stability could be even higher than the limit of a wet cell, the electrochemical stability of Li-BDS seems very good and the biggest problem still lies in the low ionic conductivity. The low conductivity presumably derives from the low degree of dissociation of the Li-ions in the structure. Typically, the sulfonate-based solid ion conductors exist as side groups in other polymer matrices where for example the polyethylene glycol can dissociate the Li-ions and act as a conductive medium rather than the strictly bound Li-sulfonate groups. However, increasing the conductivity might decrease the stability of the material. This underlines the importance to further optimize the morphologies and (crystal) structures of the conductive SPSLICs to support the higher degree of Li-ion dissociation, without sacrificing the stability, and then challenge the ALD/MLD fabrication of these materials.

Conclusion

We developed two new ALD/MLD processes for Li- and Cu-based 1,4-benzenedisulfonate coordinate compounds. Both processes yielded crystalline films with hydration water. The crystal structure of the latter films matched with previously reported bulk-synthesized hydrated Cu-BDS. The Li-BDS films were crystalline and hydrated as well, but the crystal structure could not be identified as there were no previous reports for the crystal structure of Li-BDS. The as-deposited Li-BDS films readily released the hydrated water, and remained crystalline and stable, allowing us to characterize them for the ionic conductivity; the value of $6.4\cdot10^{-8}$ S/cm reached at 118°C is low but comparable to related materials in bulk form. We foresee that with the clever tuning of the structure, mainly adding groups to dissociate the Li-ions, it could be possible to increase the ionic conductivity of these materials without obliterating the stability. This would be important to facilitate the ALD/MLD fabrication of solid polymer ionic conductors of true application relevance.

Acknowledgements
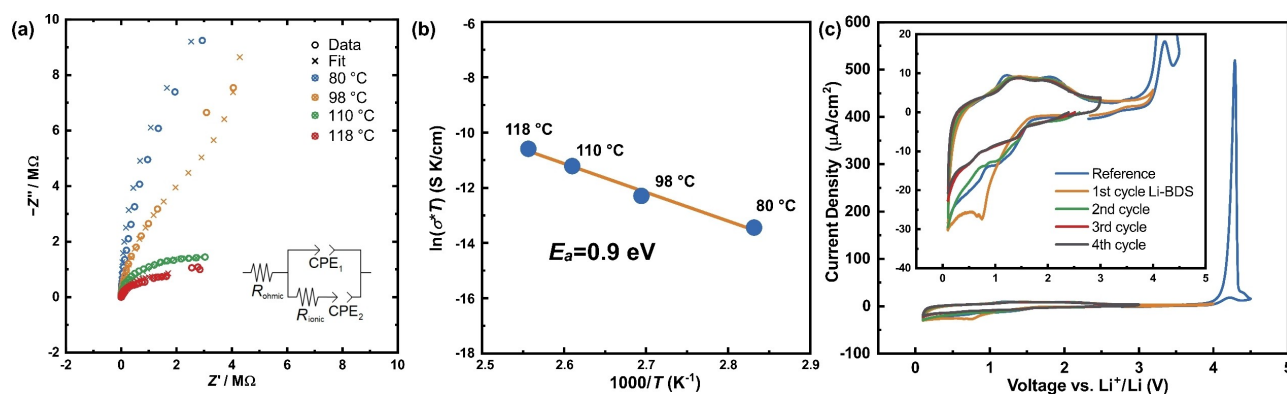
Figure 5. (a) Measured EIS spectra at different temperatures with fits and equivalent circuit, (b) Arrhenius plot of conductivity and calculated activation energy according to the linearization. (c) Cyclic voltammetry of a reference cell without a film and with 100 nm of Li-BDS film.

Conflict of Interest

The authors declare no conflict of interest.

[1] T. Suntola, J. Antson, US Pat., 4,058,430, **1977**.
[2] S. M. George, *Chem. Rev.* **2010**, *110*, 111–131.
[3] Y. Zhao, K. Zheng, X. Sun, *Joule* **2018**, *2*, 2583–2604.
[4] O. Nilsen, V. Miikkulainen, K. B. Gandrud, E. Østreng, A. Ruud, H. Fjellvåg, *Phys. Status Solidi* **2014**, *211*, 357–367.
[5] P. Sundberg, M. Karppinen, *Beilstein J. Nanotechnol.* **2014**, *5*, 1104–1136.
[6] J. Liu, H. Zhu, M. H. A. Shiraz, *Front. Energy Res.* **2018**, *6*, 1–5.
[7] J. Liu, X. Sun, *Nanotechnology* **2015**, *26*, 24001.
[8] H. C. M. Knoops, M. E. Donders, M. C. M. Van de Sanden, P. H. L. Notten, W. M. M. Kessels, *J. Vac. Sci. Technol. A* **2012**, *30*, 010801.
[9] O. Tiurin, Y. Ein-Eli, *Adv. Mater. Interfaces* **2019**, *6*, 1901455.
[10] J. Heiska, M. Nisula, M. Karppinen, *J. Mater. Chem. A* **2019**, *7*, 18735–18758.
[11] X. Meng, X.-Q. Yang, X. Sun, *Adv. Mater.* **2012**, *24*, 3589–3615.
[12] J. Heiska, M. Madadi, M. Karppinen, *Nanoscale Adv.* **2020**, *2*, 2441–2447.
[13] X. Meng, *Energy Storage Mater.* **2020**, *30*, 296–328.
[14] Y. Zhao, L. V. Goncharova, Q. Sun, X. Li, A. Lushington, B. Wang, R. Li, F. Dai, M. Cai, X. Sun, *Small Methods* **2018**, *2*, 1700417.
[15] Q. Sun, K. C. Lau, D. Geng, X. Meng, *Batter. Supercaps* **2018**, *1*, 41–68.
[16] X. Meng, *J. Mater. Chem. A* **2017**, *5*, 18326–18378.
[17] Y. Zhao, M. Amirmaleki, Q. Sun, C. Zhao, A. Codirenzi, L. V. Goncharova, C. Wang, K. Adair, X. Li, X. Yang, F. Zhao, R. Li, T. Filleter, M. Cai, X. Sun, *Matter* **2019**, *1*, 1215–1231.
[18] M. Armand, M. Duclot, P. Rigaud, *Solid State Ionics* **1981**, *3–4*, 429–430.
[19] L. Yue, J. Ma, J. Zhang, J. Zhao, S. Dong, Z. Liu, G. Cui, L. Chen, *Energy Storage Mater.* **2016**, *5*, 139–164.
[20] P. Albertus, S. Babinec, S. Litzelman, A. Newman, *Nat. Energy* **2018**, *3*, 16–21.
[21] K. Jeong, S. Park, S. Y. Lee, *J. Mater. Chem. A* **2019**, *7*, 1917–1935.
[22] M. D. Tikekar, L. A. Archer, D. L. Koch, *J. Electrochem. Soc.* **2014**, *161*, A847–A855.
[23] S. Guhathakurta, K. Min, *Polymer* **2010**, *51*, 211–221.
[24] N. Shubha, H. Zhu, M. Forsyth, M. Srinivasan, *Polymer* **2016**, *99*, 748–755.
[25] R. Rohan, Y. Sun, W. Cai, Y. Zhang, K. Pareek, G. Xu, H. Cheng, *Solid State Ionics* **2014**, *268*, 294–299.
[26] H. Wang, K. E. Gregorczyk, S. B. Lee, G. W. Rubloff, C. Lin, *J. Phys. Chem. C* **2020**, *124*, 6830–6837.
[27] E. Kazyak, M. Shin, W. S. LePage, T. H. Cho, N. P. Dasgupta, *Chem. Commun.* **2020**, *56*, 15537–15540.
[28] K. B. Lausund, V. Petrovic, O. Nilsen, *Dalton Trans.* **2017**, *46*, 16983–16992.
[29] K. B. Klepper, O. Nilsen, H. Fjellvåg, *Dalton Trans.* **2010**, *39*, 11628–11635.
[30] E. Ahvenniemi, M. Karppinen, *Chem. Commun.* **2016**, *52*, 1139–1142.
[31] A. Tanskanen, M. Karppinen, *Sci. Rep.* **2018**, *8*, 8976.
[32] J. Penttinen, M. Nisula, M. Karppinen, *Chem. Eur. J.* **2017**, *23*, 18225–18231.
[33] M. Nisula, M. Karppinen, *Nano Lett.* **2016**, *16*, 1276–1281.
[34] J. Heiska, M. Nisula, E.-L. Rautama, A. J. Karttunen, M. Karppinen, *Dalton Trans.* **2020**, *49*, 1591–1599.
[35] J. Multia, J. Heiska, A. Khayyami, M. Karppinen, *ACS Appl. Mater. Interfaces* **2020**, *12*, 41557–41566.
[36] R. Ghiyasi, G. C. Tewari, M. Karppinen, *J. Phys. Chem. C* **2020**, *124*, 13765–13770.
[37] J. P. Guthrie, *Can. J. Chem.* **1978**, *56*, 2342–2354.
[38] G. P. Panasyuk, L. A. Azarova, G. P. Budova, A. P. Savost'yanov, *Inorg. Mater.* **2007**, *43*, 951–955.
[39] A. Mietrach, T. W. T. Muesmann, J. Christoffers, M. S. Wickleder, *Eur. J. Inorg. Chem.* **2009**, *2009*, 5328–5334.
[40] P. M. Shanthi, P. J. Hanumantha, K. Ramalinga, B. Gattu, M. K. Datta, P. N. Kumta, *J. Electrochem. Soc.* **2019**, *166*, A1827–A1835.
[41] A. E. Lakraychi, E. Deunf, K. Fahsi, P. Jimenez, J.-P. P. Bonnet, F. Djedaini-Pilard, M. Bécuwe, P. Poizot, F. Dolhem, *J. Mater. Chem. A* **2018**, *6*, 19182–19189.
[42] J. Penttinen, M. Nisula, M. Karppinen, *Chem. Eur. J.* **2019**, *25*, 11466–11473.
[43] A. Ghazy, M. Safdar, M. Lastusaari, M. Karppinen, *Chem. Commun.* **2020**, *56*, 241–244.
[44] D. D. Jiang, Q. Yao, M. A. McKinney, C. A. Wilkie, *Polym. Degrad. Stab.* **1999**, *63*, 423–434.
[45] N. M. Shishlov, S. L. Khursan, *J. Mol. Struct.* **2016**, *1123*, 360–366.
[46] E. Kazyak, K. Chen, A. L. Davis, S. Yu, A. J. Sanchez, J. Lasso, A. R. Bielinski, T. Thompson, J. Sakamoto, D. J. Siegel, N. P. Dasgupta, *J. Mater. Chem. A* **2018**, *6*, 19425–19437.
[47] R. A. Huggins, *Ionics* **2002**, *8*, 300–313.